# Reduction of Residual Vibration in Displacement-Amplified Micro-Electromagnetic Actuators with Non-linear Dynamics Using Input Shaping

Gerald Eaglin[1], Joshua Vaughan[1], and Hiroyuki Nabae[2]

***Abstract*— Micro-electromagnetic actuators have been used in many fields and industries for systems such as microfluidic systems, positioning stages, and robotic manipulators. Small-scale electromagnetic actuators are able to provide rapid motion with high positioning accuracy. The actuator presented in this paper utilizes a displacement amplification mechanism to increase the maximum stroke length that can be achieved. The dynamics of this actuator are nonlinear due to the dependence of the applied force on gap distance between the coils and the amplification mechanism. This nonlinearity causes the performance of PID control to vary with respect to the displacement of the actuator. The control method proposed in this paper to limit the overshoot resulting from nonlinearity uses a combination of PID control and robust input shapers. Using robust input shapers to account for parameter variation across the workspace, the combined controller eliminates the overshoot while maintaining short settling times. Simulations are presented to demonstrate the performance of the proposed method.**

## I. Introduction

There are various types of micro-electromagnetic actuators that are used for a variety of applications in industry and research. A few of the main application areas of small-scale actuators include microfluidic systems, positioning systems, and robotic manipulators [1]. Advantages of using electromagnetic actuators for these applications include short rise time and low input-voltage [2]. Solid-state actuators, such as piezoelectric actuators, are also capable of rapid motion for micro-scale applications. However, they typically provide stroke distances that are shorter than micro-electromagnetic actuators [3], [4]. Similarly, electrostatic actuators provide rapid motion, but require high voltage-inputs in order to achieve large displacements and are sensitive to airborne particulates [2], [5].

The actuator addressed in this paper has nonlinear dynamics dependent on its displacement. Methods that have been used to account for nonlinear dynamics of electromagnetic actuators include using linear parameter-varying models in conjunction with a robust, gain-scheduled controller [6]. PID control, quadratic feedback control, and optimal feedback control have been used for vibration control of a cantilever beam with a tip mass [7]. An inverse-Preisach-model-based feedforward sliding-mode controller has also been used to control a micro-positioning stage driven by electromagnetic actuators [4].

Because of the nonlinear dynamics of the actuator discussed in this paper, the response characteristics with a PID controller are related to its displacement, which results in overshoot for setpoints higher than the setpoint about which the PID gains were tuned. In this paper, a method is proposed to mitigate overshoot by combining PID control with input shaping. Input shaping has been used to reduce the residual vibration amplitude of flexible systems [8]–[11]. When combined with feedback controllers, it has the potential to improve both rise time and settling time of the system while canceling residual vibration. Combined feedback and input shaping controllers can also provide robustness to sensor disturbances and discontinuous nonlinearities [10], [12]. In this work, the use of input shaping combined with PID control allows the actuator to retain a fast response time while limiting overshoot and residual vibration over the entire workspace.

The next section introduces the actuator and its model used for simulation. Section III then discusses the closed-loop dynamics of the actuator subject to PID control and explains how its nonlinearity affects the performance. Section IV gives an overview of input shaping followed by a discussion of tuning of the combined controller and selection of the input shaper. Lastly, Section V analyzes the performance of the combined controller and compares the results with PID control.

## II. Model of Micro-Electromagnetic Actuator

The simulations presented in this paper were performed using a model of the actuator shown in Figure 1 [13]. This actuator uses a displacement amplification mechanism to increase the maximum stroke length that can be achieved and reduce the necessary current output [13], [14]. When current is applied to the coils of the actuator, the size of the gap decreases, pushing out the amplification mechanism. For this actuator, the amplification mechanism is designed to provide an amplification ratio approximately equal to four. The equation of motion describing the dynamics of this system is [13]:

$$\frac{M_0}{A}\ddot{x}_{out} + \frac{C_0}{A}\dot{x}_{out} + \frac{K_0}{A}x_{out} = F_{in} \tag{1}$$

This work was supported by the NSF EAPSI program (No. 1714043), the research-aid fund of the Mitsutoyo Association for Science and Technology, the Louisiana Board of Regents, and HiBot

[1]Gerald Eaglin and Joshua Vaughan are with the Department of Mechanical Engineering, University of Louisiana at Lafayette, LA 70503, USA joshua.vaughan@louisiana.edu

[2]Hiroyuki Nabae is with the Department of Mechanical Engineering, Tokyo Institute of Technology, Meguro, Tokyo 152-8550, Japan nabae@mes.titech.ac.jp

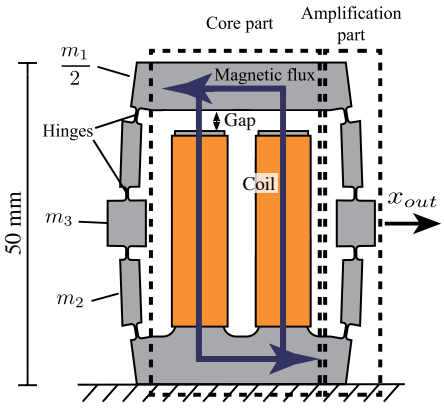


Fig. 1. Micro-electromagnetic actuator utilizing a displacement amplification mechanism [13]

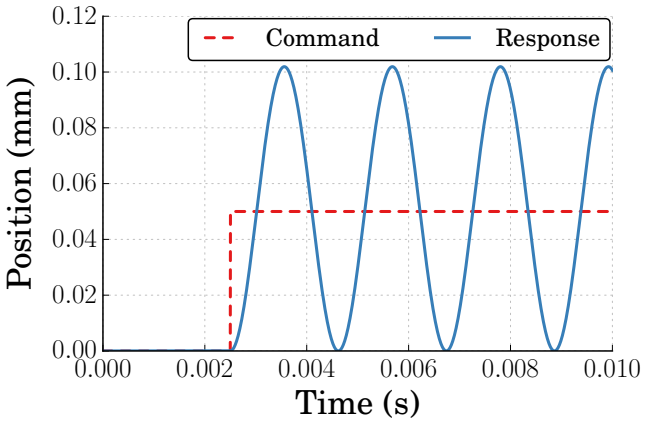


Fig. 2. Open-loop, undamped response of the actuator

where $M_0$ is the effective mass, $C_0$ is the damping coefficient, $K_0$ is the stiffness, $A$ is the amplification ratio, $x_{out}$ is the displacement of the output as shown in Figure 1, and $F_{in}$ is the force input. The effective mass, $M_0$, and the stiffness, $K_0$, are defined by:

$$M_0 = \frac{12m_1 + \left(15 + 4A^2\right) m_2 + 6\left(1 + A^2\right) m_3}{3} \tag{2}$$

$$K_0 = \frac{8K_r A^2}{l_a^2} \tag{3}$$

where $K_r$ and $l_a$ are the rotational elastic moduli and length of each hinge, respectively. The damping coefficient, $C_0$, was determined experimentally. The force input, $F_{in}$, is defined by:

$$F_{in} = \frac{\alpha I^2}{\left(\bar{x} + x_g\right)^2} \tag{4}$$

where $I$ is the applied current, and $\bar{x}$ is a function of the magnetic permeability of the components of the actuator. The gap width, $x_g$, and $\alpha$ are defined by:

$$x_g = x_{g0} - \frac{x_{out}}{A} \tag{5}$$

$$\alpha = 4\mu_0 S N^2 \tag{6}$$

where $\mu_0$ is the space permeability, $S$ is the cross-sectional area of the gap, $N$ is the number of turns of the coil, and $x_{g0}$ is the initial gap width. The applied force is a function of not only the applied current, but also the displacement of the actuator, contributing to the nonlinear dynamics. A more detailed explanation of the derivation and verification of this equation of motion can be found in [13].

The open-loop, undamped response of the actuator is shown in Figure 2, where the current necessary to achieve a setpoint, $x_{des}$, of 0.05mm was calculated using:

$$I^2 = \frac{K_0 x_{des}\left(\bar{x} + x_{g,des}\right)^2}{A\alpha} \tag{7}$$

where $x_{g,des}$ is the gap distance at $x_{des}$. When this current is applied to the system, the command induces residual vibration. Feedback can be used to control the actuator and reduce residual vibration, as will be shown in the next section.

## III. Analysis of Closed-Loop Dynamics

### A. Closed-Loop Equation of Motion

To analyze the closed-loop dynamics of the actuator, $I^2$ is used as the PID output. While the open-loop dynamics are second-order, the use of integral gain results in a third-order closed-loop transfer function. The equation of motion of the closed-loop system is:

$$\dddot{\Gamma} = -\left(\frac{A\alpha}{M_0 r} K_I\right)\Gamma - \left(\frac{A\alpha}{M_0 r} K_p + \frac{K_0}{M_0}\right)\dot{\Gamma} - \left(\frac{A\alpha}{M_0 r} K_d + \frac{C_0}{M_0}\right)\ddot{\Gamma} + u \tag{8}$$

where $\Gamma$ is the integral of displacement with respect to time, and $K_p$, $K_I$, and $K_d$ are the proportional, integral, and derivative gains, respectively, and $u$ is defined by:

$$u = \frac{A\alpha}{M_0 r}\left(K_I \Gamma_{des} + K_p \dot{\Gamma}_{des} + K_d \ddot{\Gamma}_{des}\right) \tag{9}$$

where $\Gamma_{des}$ is the integral with respect to time of the desired displacement. In both (8) and (9), $r$ is a function of $\bar{x}$, $x_{g0}$, and the displacement of the actuator, which is defined as:

$$r = \left(\bar{x} + x_{g0} - \frac{\dot{\Gamma}}{A}\right)^2 \tag{10}$$

To determine how the behavior of the actuator changes with respect to its displacement, (8) was linearized about a sequence of displacements so that the pole locations can be found. This is done by evaluating (10) at each displacement, which then becomes:

$$r_0 = \left(\bar{x} + x_{g0} - \frac{\dot{\Gamma}_{des}}{A}\right)^2 \tag{11}$$

Figure 3 shows the poles of the actuator when linearized about displacements ranging from 0 to 0.1mm while using

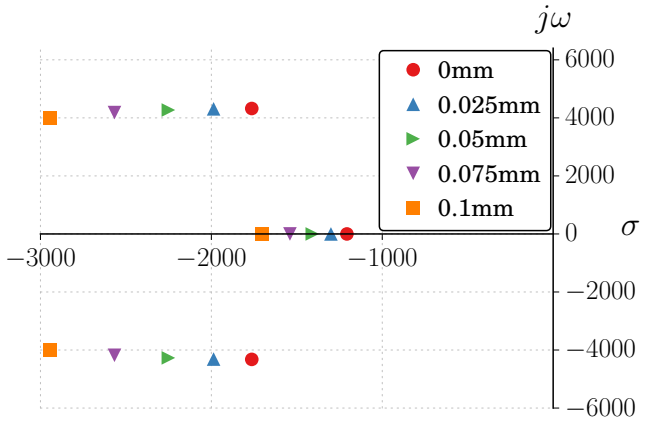


Fig. 3. Poles for desired setpoints of 0, 0.025mm, 0.05mm, 0.75mm, and 0.1mm

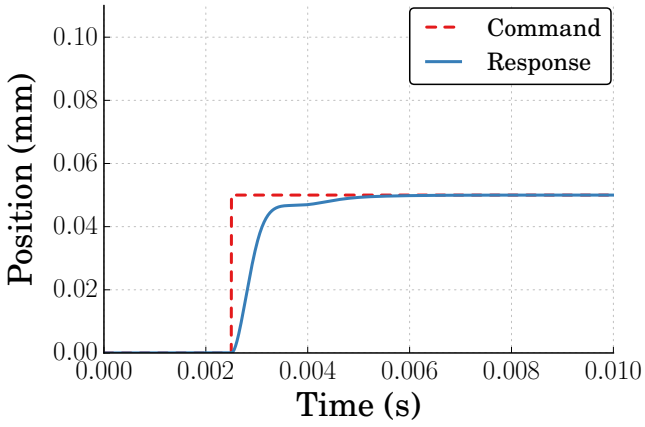


Fig. 4. Performance of the PID controller for a setpoint of 0.05mm

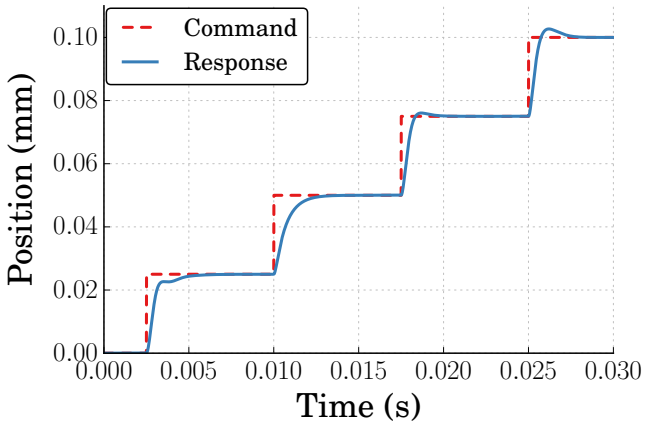


Fig. 5. Performance of the PID controller for a stair-step command

PID gains of $K_p = 1.8$, $K_I = 3334$, and $K_d = 6 \times 10^{-4}$. The nonlinearity can be observed by the movement of the poles as displacement changes. As displacement increases, the first-order poles move to the left, increasing the decay rate of the first-order response. The frequency and damping ratio of the second-order poles also increase.

### B. Performance under PID Control

Before analyzing the performance of the combined PID and input shaping controller, simulations of a PID controller are presented for comparison. The gains were tuned using a step command from 0 to 0.05mm, which is half of the maximum stroke length. The twiddle method was used to minimize a cost function:

$$J = \alpha\,(PO)^2 + \beta T_s^2 \tag{12}$$

where $PO$ is the percent overshoot and $T_s$ is the settling time of the response. The gains that minimize the cost function are $K_p = 1.8$, $K_I = 3334$, and $K_d = 6 \times 10^{-4}$. The response of the actuator to a step command from 0 to 0.05mm is shown in Figure 4, where the response has a settling time of $2.10 \times 10^{-3}$s and no overshoot.

Because of the nonlinearity, the performance of the PID controller is inconsistent for command profiles different from that for which it was tuned, as shown for the stair-step command profile in Figure 5. For instance, although the response in Figure 4 does not have overshoot, the steps at 0.075mm and 0.1mm in Figure 5 have percent overshoot of 4.3% and 10.7%, respectively. The response characteristics of the PID controller for the stair-step command are summarized in Table I.

## IV. PID Control and Input Shaping

### A. Input Shaping Overview

Input shaping limits residual vibration by convolving a sequence of impulses with a reference command to reduce the vibration amplitude of a response [8], [15]. An illustration of the input shaping process for a Zero Vibration (ZV) shaper is shown in Figure 6. When the original unshaped reference command is passed to the system, it induces vibration. The two impulses of the input shaper are convolved with the reference command to produce a shaped command that results in zero residual vibration. As a consequence of the convolution process, the duration of the shaped command is longer than that of the original command by an amount equal to the time of the last impulse of the shaper, which is $\Delta$ in Figure 6.

The necessary impulse amplitudes and time locations that are convolved with the shaper to limit unwanted oscillation are found using constraints on residual vibration amplitude and the input shaper impulse amplitudes and times. The amplitude of the residual vibration response resulting from

TABLE I
PID Response Characteristics

| Step | % Overshoot | 5% Settling Times (s) |
|---|---|---|
| 0–0.025mm | 0 | $2.03 \times 10^{-3}$ |
| 0.025–0.05mm | 0 | $2.04 \times 10^{-3}$ |
| 0.05–0.075mm | 4.3% | $7.3 \times 10^{-4}$ |
| 0.075–0.1mm | 10.7% | $1.93 \times 10^{-3}$ |

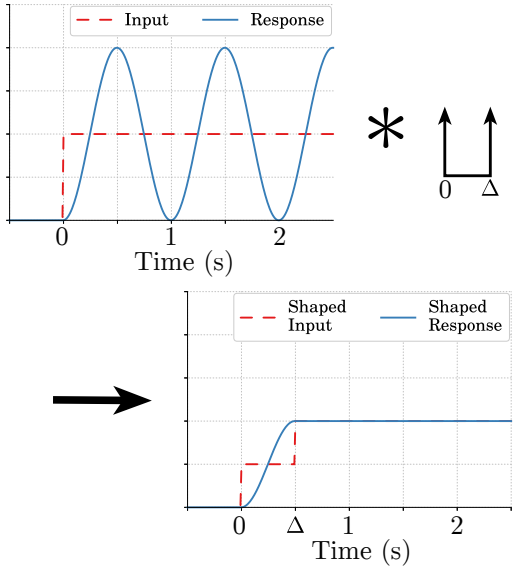


Fig. 6. Convolution of a ZV shaper with a step command

a sequence of $n$ impulses normalized by the response which results from a unity magnitude impulse at time zero is [8]:

$$V(\omega,\zeta) = e^{-\zeta\omega t_n}\sqrt{[C(\omega,\zeta)]^2 + [S(\omega,\zeta)]^2} \tag{13}$$

where

$$C(\omega,\zeta) = \sum_{i=1}^{n} A_i e^{\zeta\omega t_i}\cos\left(\omega t_i\sqrt{1-\zeta^2}\right) \tag{14}$$

$$S(\omega,\zeta) = \sum_{i=1}^{n} A_i e^{\zeta\omega t_i}\sin\left(\omega t_i\sqrt{1-\zeta^2}\right) \tag{15}$$

and $\zeta$ is the damping ratio of the system, $\omega$ is the natural frequency, and $A_i$ and $t_i$ are the $i^{th}$ impulse amplitude and time location. This is known as the percent residual vibration (PRV) and is used to measure the residual vibration amplitude produced by the shaped command over the amplitude produced by the unshaped command. This equation is used to form a constraint by setting it less than or equal to a tolerable level of residual vibration, $V_{tol}$. To ensure that the shaped command reaches the same set-point as the unshaped command, impulse amplitudes are constrained to sum to one. The time of the last impulse, $t_n$, is then minimized to ensure the shortest input shaper duration.

The above constraints are common to all types of input shapers. Additional constraints are needed depending on the type of input shaper desired. For instance, for the ZV-shaper shown in Figure 6, $V_{tol}$ is set to zero, and each impulse amplitude is constrained to be greater than zero.

The robustness of input shapers to error in natural frequency is quantified using Insensitivity. The sensitivity curves of various shapers are shown in Figure 7, where the percent residual vibration is plotted on the vertical axis and actual frequency normalized by the modeled frequency is plotted on the horizontal axis. For a desired $V_{tol}$, the Insensitivity of a shaper is the range of normalized frequency for

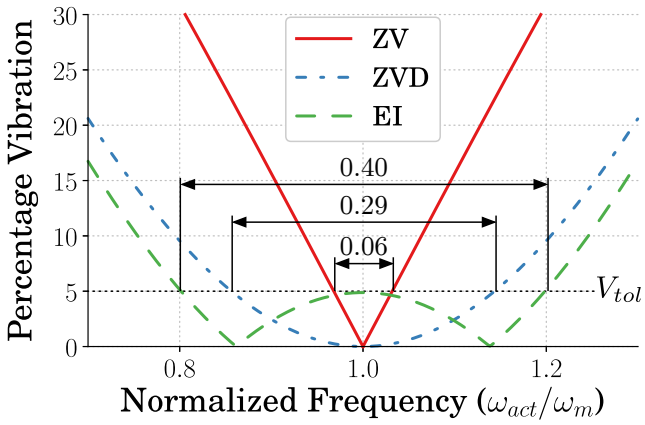


Fig. 7. Sensitivity curves of ZV, ZVD, and EI shapers

which the sensitivity curve falls below $V_{tol}$. The robustness of input shaping can be increased by including additional robustness constraints. However, typically shaper duration also increases as shaper robustness increases, where longer shaper duration usually results in longer response rise time [16].

### *B. PID Tuning for Input Shaping*

Because (13) is derived for the response of a second-order, underdamped system, the PID controller is retuned so that the second-order poles are dominant. When the system is oscillatory, the sum of the coefficients for $\Gamma$ and $\Gamma_{des}$ is nearly zero such that (8) can be simplified to approximate a second-order system, and the natural frequency and damping ratio are described by:

$$w = \sqrt{\frac{A\alpha}{M_0 r}K_p + \frac{K_0}{M_0}} \tag{16}$$

$$\zeta = \frac{1}{2\omega_n}\left(\frac{A\alpha}{M_0 r}K_d + \frac{C_0}{M_0}\right) \tag{17}$$

where both (16) and (17) are functions of actuator displacement due to $r$, so that the natural frequency and damping ratio vary over the workspace of the actuator. The negative effects of this nonlinearity on the performance of input shaping can be reduced by using piecewise and energy-based shaper designs, as well as using robust input shapers [17]–[19].

As proportional gain increases, the median and range of (16) across the workspace also increase. The range of natural frequency normalized by the median frequency represents the Insensitivity required by the input shaper in order to limit residual vibration below the tolerable level. Figure 8 shows the required Insensitivity verses a range of proportional gains to suppress vibration for frequencies between displacements of 0 and 0.1mm. Once the value of $K_p$ is chosen, a Specified Insensitivity (SI) input shaper can be designed to mitigate residual vibration within the necessary frequency range. In addition to constraining impulse amplitudes to sum to one, SI shapers limit vibration over an arbitrary range of frequency

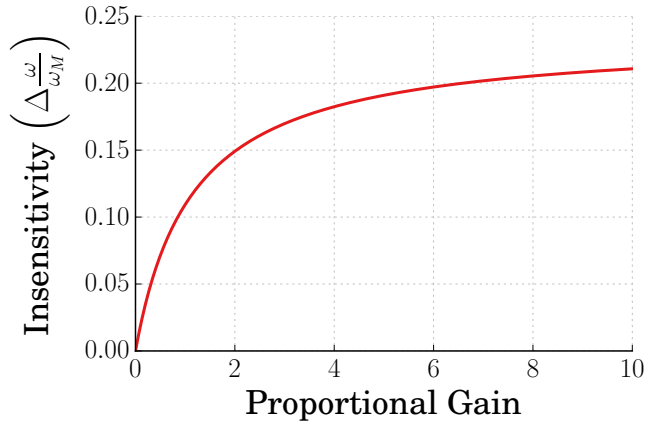


Fig. 8. Required Insensitivity across actuator workspace for a range of proportional gains

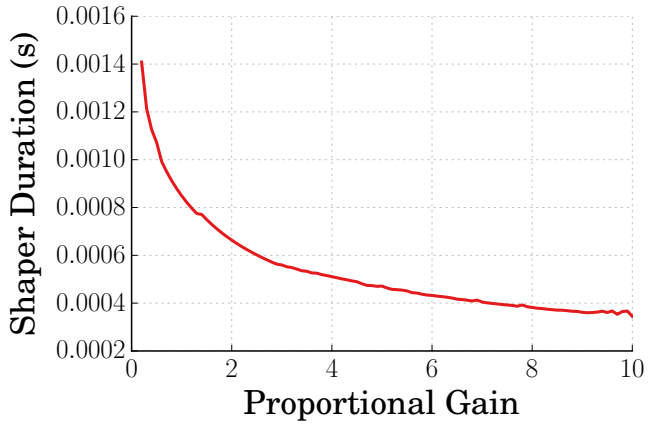


Fig. 9. Duration of SI input shaper for a range of proportional gains

by constraining (13) less than or equal to $V_{tol}$ for sampled frequencies within the desired range [20]:

$$V\left(\omega_k, \zeta\right) \leq V_{tol}, \quad \forall \omega_k \in [\omega_1, \omega_2] \tag{18}$$

where $\omega_1$ and $\omega_2$ are the bounds of the desired frequency range, and $\omega_k$ is the $k^{th}$ sampled frequency in that range. For the actuator, $\omega_1$ and $\omega_2$ are the values of (16) at displacements of 0 and $0.1\text{mm}$, respectively, for a given $K_p$.

Increasing the Insensitivity of an input shaper typically results in longer shaper durations. Although the use of higher proportional gains increases the range of (16) and requires shapers with higher Insensitivity, the increase in median natural frequency allows for faster rise times, resulting in shorter shaper durations. This is shown in Figure 9 where the duration of an SI shaper tends to decrease as proportional gain increases. Due to this, a high natural frequency is achieved by using the highest possible proportional gain, which limits the delay introduced by input shaping. The PID controller then provides a fast rise time while the input shaper reduces the overshoot and residual vibration induced by the command.

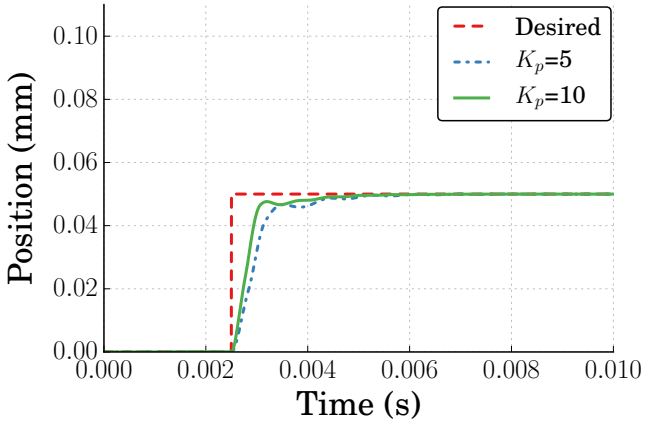


Fig. 10. Performance of the combined controller for a setpoint of $0.05\text{mm}$

## V. Performance of Combined Controller

Two sets of PID gains were chosen for the combined controller to compare its performance to PID control alone. The first set of gains used is $K_p = 5$, $K_I = 10594$, and $K_d = 2.10 \times 10^{-4}$. The impulse amplitudes and times of the SI input shaper used for these gains are:

$$\text{SI}_{K_p=5} = \begin{bmatrix} A_i \\ t_i \end{bmatrix} = \begin{bmatrix} 0.3902 & 0.4392 & 0.1706 \\ 0.0 & 0.0004 & 0.0007 \end{bmatrix} \tag{19}$$

The second set of gains used for the combined controller is $K_p = 10$, $K_I = 20000$, and $K_d = 2.25 \times 10^{-4}$. These gains are utilized with the SI input shaper with impulse amplitudes and times of:

$$\text{SI}_{K_p=10} = \begin{bmatrix} A_i \\ t_i \end{bmatrix} = \begin{bmatrix} 0.3621 & 0.4504 & 0.1875 \\ 0.0 & 0.0003 & 0.0005 \end{bmatrix} \tag{20}$$

The responses of the controller with these gains for a setpoint of $0.05\text{mm}$ is shown in Figure 10. Both sets of gains produce no overshoot while providing settling times of $1.68 \times 10^{-3}\text{s}$ and $1.18 \times 10^{-3}\text{s}$ for $K_p = 5$ and $K_p = 10$, respectively.

Figure 11 shows the response of the combined controller for a stair-step command from setpoints of 0 to $0.1\text{mm}$. Comparing the response of the PID controller shown in Figure 5 to the combined controller, the combined controller does not produce overshoot at any setpoint while maintaining short settling times. The settling times for $K_p = 5$ and settling time normalized by the settling times using PID control alone are summarized in Table II. The combined controller reduces the settling time for each step except for the step from $0.05\text{mm}$ to $0.075\text{mm}$. Similarly, the response characteristics for $K_p = 10$ are summarized in Table III. The combined controller with $K_p = 10$ has lower settling times than the other controllers, which was expected due to having higher natural frequencies across the workspace.

A drawback of using higher proportional gains is that the peak current at the initiation of the command is higher. Using PID alone, which had the lowest proportional gain, the peak current was $0.30\text{A}$. The peak current output for $K_p = 5$ was $0.31\text{A}$ while the peak current output for $K_p = 10$ was $0.42\text{A}$.

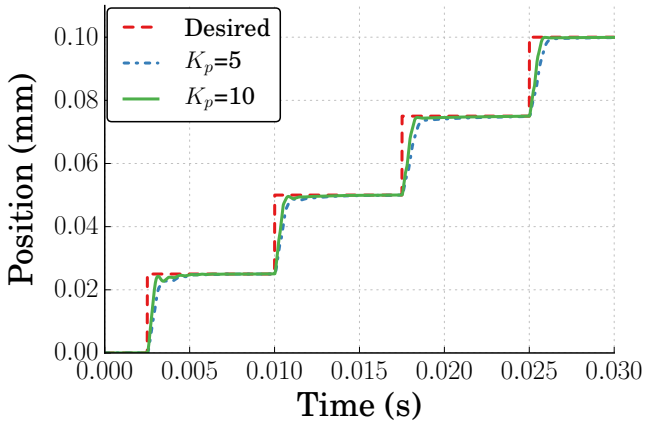


Fig. 11. Performance of the combined controller for a stair-step command

TABLE II
COMBINED CONTROLLER ($K_p = 5$) 5% SETTLING TIMES

| **Step** | **5% Settling Times** (s) | **Normalized** |
|---|---|---|
| 0–0.025mm | $1.78 \times 10^{-3}$ | 0.88 |
| 0.025–0.5mm | $1.75 \times 10^{-3}$ | 0.86 |
| 0.05–0.075mm | $1.45 \times 10^{-3}$ | 1.99 |
| 0.075–0.1mm | $1.10 \times 10^{-3}$ | 0.57 |

TABLE III
COMBINED CONTROLLER ($K_p = 10$) 5% SETTLING TIMES

| **Step** | **5% Settling Times** (s) | **Normalized** |
|---|---|---|
| 0–0.025mm | $1.19 \times 10^{-3}$ | 0.59 |
| 0.025–0.5mm | $6.64 \times 10^{-4}$ | 0.33 |
| 0.05–0.075mm | $7.43 \times 10^{-4}$ | 1.02 |
| 0.075–0.1mm | $7.23 \times 10^{-4}$ | 0.37 |

Due to this, maximum current output of the current source is the limiting factor in choosing the proportional gain for the controller.

## VI. CONCLUSION

A combined PID and input shaping controller was used to limit the overshoot and vibration amplitude of a micro-electromagnetic actuator with nonlinear dynamics. It was shown that the nonlinearity caused the performance of the actuator with PID control alone to vary depending on its displacement. This contributed to overshoot for high set-points. The natural frequency of the actuator increases with proportional gain, providing faster rise times and allowing for shorter shaper durations despite the need for shapers with more robustness. The combined PID and input shaping controller exploits this property and eliminates overshoot while maintaining short settling times.

## ACKNOWLEDGMENT

The authors would like to thank Professor Endo of the Suzumori-Endo Lab at Tokyo Institute of Technology for serving as a host for this work to be conducted.

## REFERENCES

[1] S. Büttgenbach, "Electromagnetic micromotors—design, fabrication and applications," *Micromachines*, pp. 929–942, October 2014.
[2] H. Guckel, T. Earles, J. Klein, J. Zook, and T. Ohnstein, "Electromagnetic linear actuators with inductive position sensing," *Sensors and Actuators A: Physical*, vol. 53, no. 1, pp. 386 – 391, 1996.
[3] Z. Qiu, J. S. Pulskamp, X. Lin, C.-H. Rhee, T. Wang, R. G. Polcawich, and K. Oldham, "Large displacement vertical translational actuator based on piezoelectric thin films," *Journal of Micromechanics and Microengineering*, vol. 20, no. 7, 2010.
[4] S. Xiao and Y. Li, "Optimal design, fabrication, and control of an $xy$ micropositioning stage driven by electromagnetic actuators," *IEEE Transactions on Industrial Electronics*, vol. 60, no. 10, pp. 4613–4626, Oct 2013.
[5] J. D. Grade, H. Jerman, and T. W. Kenny, "Design of large deflection electrostatic actuators," *Journal of Microelectromechanical Systems*, vol. 12, no. 3, pp. 335–343, June 2003.
[6] A. Forrai, T. Ueda, and T. Yumura, "Electromagnetic actuator control: A linear parameter-varying (lpv) approach," *IEEE Transactions on Industrial Electronics*, vol. 54, no. 3, pp. 1430–1441, June 2007.
[7] R.-F. Fung, Y.-T. Liu, and C.-C. Wang, "Dynamic model of an electromagnetic actuator for vibration control of a cantilever beam with a tip mass," *Journal of Sound and Vibration*, vol. 288, no. 4, pp. 957 – 980, 2005.
[8] N. C. Singer and W. P. Seering, "Preshaping command inputs to reduce system vibration," *Journal of Dynamic Systems, Measurement, and Control*, vol. 112, pp. 76–82, March 1990.
[9] W. Singhose, W. Seering, and N. Singer, "Residual vibration reduction using vector diagrams to generate shaped inputs," *Journal of Mechanical Design*, vol. 116, no. 2, pp. 654–659, 06 1994.
[10] J. Huey and W. Singhose, "Design of proportional-derivative feedback and input shaping for control of inertia plants," *Control Theory Applications, IET*, vol. 6, no. 3, pp. 357–364, 2012.
[11] W. Singhose, "Command shaping for flexible systems: A review of the first 50 years," *International Journal of Precision Engineering and Manufacturing*, vol. 10, no. 4, pp. 153–168, 2009.
[12] J. R. Huey, K. L. Sorensen, and W. E. Singhose, "Useful applications of closed-loop signal shaping controllers," *Control Engineering Practice*, vol. 16, no. 7, pp. 836 – 846, 2008.
[13] H. Nabae and T. Higuchi, "A novel electromagnetic actuator based on displacement amplification mechanism," *IEEE/ASME Transactions on Mechatronics*, vol. 20, no. 4, pp. 1607–1615, Aug 2015.
[14] H. Zhou and B. Henson, "Analysis of a diamond-shaped mechanical amplifier for a piezo actuator," *The International Journal of Advanced Manufacturing Technology*, vol. 32, no. 1-2, pp. 1–7, 2007.
[15] O. Smith, "Posicast control of damped oscillatory systems," *Proceedings of the IRE*, vol. 45, no. 9, pp. 1249–1255, 1957.
[16] J. Vaughan, A. Yano, and W. Singhose, "Comparison of robust input shapers," *Journal of Sound and Vibration*, vol. 315, no. 4-5, pp. 797 – 815, 2008.
[17] E. Crain, W. Singhose, and W. Seering, "Evaluation of input shaping on configuration dependent systems," in *Japan-USA symposium of flexible automation, Boston, MA*, 1996.
[18] J. Y. Smith, K. Kozak, and W. E. Singhose, "Input shaping for a simple nonlinear system," in *Proceedings of the 2002 American Control Conference (IEEE Cat. No.CH37301)*, vol. 1, May 2002, pp. 821–826.
[19] K.-S. Chen, T.-S. Yang, K.-S. Ou, and J.-F. Yin, "Design of command shapers for residual vibration suppression in duffing nonlinear systems," *Mechatronics*, vol. 19, no. 2, pp. 184 – 198, 2009.
[20] W. E. Singhose, W. P. Seering, and N. C. Singer, "Input shaping for vibration reduction with specified insensitivity to modeling errors," in *Japan-USA Sym. on Flexible Automation*, 1996.